ACS APPLIED MATERIALS & INTERFACES

Research Article

Cite This: ACS Appl. Mater. Interfaces 2019, 11, 33676−33683

www.acsami.org

Perylene Diimide and Luminol as Potential-Resolved Electrochemiluminescence Nanoprobes for Dual Targets Immunoassay at Low Potential

Yue Song,[†] Wei Zhang,*[,†] Shuijian He,[‡] Lei Shang,[†] Rongna Ma,[†] Liping Jia,[†] and Huaisheng Wang*[,†]

[†]Department of Chemistry, Liaocheng University, Liaocheng 252059, China

[‡]College of Materials Science and Engineering, Nanjing Forestry University, Nanjing 210037, China

Supporting Information

ABSTRACT: In the field of clinical diagnosis, it is important to construct a potential-resolved multiplex electrochemiluminescence (ECL) biosensor for decreasing the false-positive rate and improving the diagnostic accuracy. However, the shortage of low-potential cathodic luminophores between −1 and 0 V (vs Ag/AgCl) severely limited the development of the biosensor. Herein, we synthesized a novel luminophore *N*,*N*-bis-(3-dimethyl aminopropyl)-3,4,9,10-perylene tetracarboxylic acid diimide (PDI), which gave dual emissions at −0.25/−0.26 V with $K_2S_2O_8$ as a co-reactant in aqueous solution. The ECL was assigned to excited J-type PDI dimers. Then, PDI and luminol were used as luminophores to respectively combine with graphite oxide and gold nanoparticles and form potential-resolved ECL nanoprobes. Also, this potential-resolved ECL nanoprobes were respectively functionalized by secondary antibodies (Ab_2) to construct a low-potential sandwiched ECL immunosensor for tumor markers carcinoembryonic antigen (CEA) and α-fetoprotein (AFP) simultaneous determination during linear scanning potential range from −0.6 to 0.6 V. The prepared multiplex immunosensor exhibited sensitive ECL response for CEA at −0.6 V due to PDI and that for AFP at 0.6 V due to luminol, and both linear semilogarithmical ranges were from 0.1 pg to 1 ng mL^{-1}. In addition, PDI with dual ECL peaks showed enticing prospect of built-in self-calibration for a precise quantitative and bioimaging analysis.

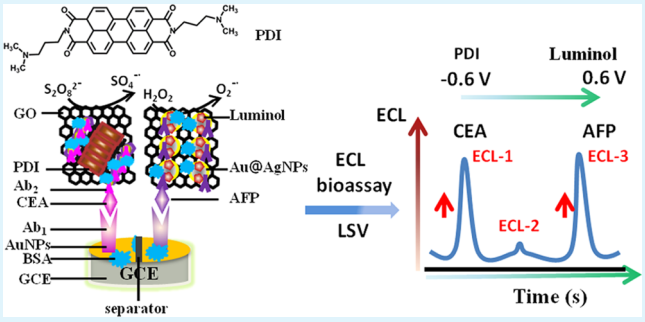

KEYWORDS: *low-potential cathodic electrochemiluminescence, multiplex immunosensor, tumor markers, perylene diimide, luminol*

1. INTRODUCTION

Electrochemiluminescence (ECL) technique has got wide application in the field of biosensing[1−4] because of its low background interference, rapid response, and high sensitivity. Highly efficient ECL nanomaterial played an important role in improving the biosensor's sensitivity.[5] Lots of interesting cathodic luminophores[6−8] such as perylenetetracarboxylic acid[9] have been reported to emit strong ECL and used to prepare ECL nanomaterials for constructing biosensors. However, these cathodic luminophores need a highly negative ECL potential (more than −1.2 V, some even at −2 V vs Ag/AgCl) to produce a strong ECL. At such a high potential, oxygen in the electrolyte also can produce emission,[10] which caused a background signal for the biosensor and decreased its sensitivity. Lowering the ECL potential of luminophores could avoid the oxygen emission. However, few low-potential ECL system have been reported.[11,12] Thus, it is essential to design low-potential luminophores for constructing sensitive ECL biosensors.

In the field of clinical diagnosis, it is important to construct sensitive multiplex biosensors[13] for decreasing the false-positive rate and improving the diagnositic accuracy. Multiplex ECL biosensors[14−16] highly demanded spectrum-resolved luminophores or potential-resolved luminophores.[17] Some spectrum-resolved luminophores such as carbon nitride nanosheets gold nanoparticles (CNNS-AuNPs) (435 nm), sulfur-doped CNNS-AuNPs (531 nm),[18] CdSe (550 nm), CdTe (650 nm), and CdTe (776 nm) nanocrystals[19] have been developed to fabricate the multiplex ECL biosensors. The spectrum-resolved multiplex ECL biosensors need a highly accurate spectrometer to record the ECL spectrum signal, which required a high sample detection cost. Potential-resolved multiplex ECL biosensors did not need a spectrometer and decreased the sample detection cost. Therefore, designing potential-resolved multiplex ECL biosensors is essential. Cathodic luminophores such as CQDs and anodic luminophores such as luminol[16] and Ru-related complexes[17] were often taken as potential-resolved luminophores for fabricating multiplex ECL biosensors. Because the ECL potential of cathodic luminophores was highly negative as mentioned

Received: June 30, 2019
Accepted: August 21, 2019
Published: August 21, 2019

DOI: 10.1021/acsami.9b11416
ACS Appl. Mater. Interfaces 2019, 11, 33676−33683

Scheme 1. (a) PDI's Molecular Structure and Dual ECL Emissions at −0.25 in Cathodic Process and −0.26 V in Anodic Process. (b) Potential-Resolved ECL Nanomaterial−Antibody Conjugates' Fabrication. (c) Multiplex Immunosensor's Fabrication and Detection for CEA at −0.6 V and AFP at 0.6 V

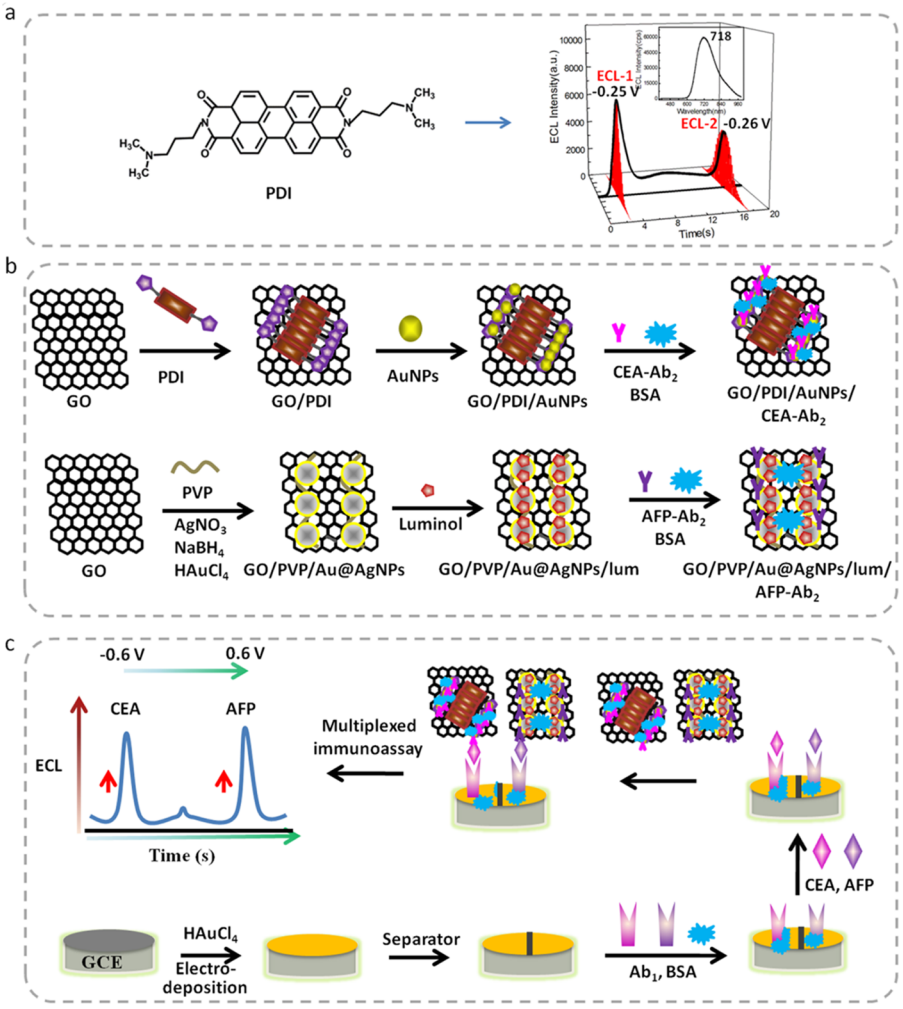

above, low-potential cathodic luminophores are fabricated that are able to increase the choice of potential-resolved luminophores and facilate the development potential-resolved multiplex ECL biosensors.

In this work, we synthesized a novel low-potential cathodic luminophore *N*,*N*-bis-(3-dimethyl aminopropyl)-3,4,9,10-perylene tetracarboxylic acid diimide (PDI) (structure shown in Scheme 1a) whose synthesis process and ^{1}H NMR spectra are shown in Scheme S1 and Figure S1. PDI displayed strong dual emissions at −0.25/−0.26 V with $K_2S_2O_8$ as a co-reactant in the aqueous system during the cycle potential range from −1 to 0 V (Scheme 1a), and its possible ECL scheme is discussed. In anodic ECL system, luminol is an low-potential luminophore at 0.6 V with H_2O_2 as a co-reactant. Thus, PDI/$S_2O_8^{2-}$ and luminol/H_2O_2 were chosen as low-potential ECL system, and dual tumor markers carcinoembryonic antigen (CEA) and α-fetoprotein (AFP) were used as model analytes in this work. Due to the large surface area, graphite oxide (GO) was used as nanocarrier to load PDI and luminol and then combined with the secondary antibodies (Ab_2) of CEA and AFP as potential-resolved ECL nanoprobes. The preparation process is shown in Scheme 1b. The polished glassy carbon electrode (GCE) was immersed into a $HAuCl_4$ solution for electrodepositing AuNPs film. After that, a slender tape of 1 mm width was pasted in the middle of GCE/AuNPs surface, which separated the electrode surface into two spatially resolved parts to effectively eliminate the interference of the potential-resolved ECL nanprobes. Two parts were used to immobilize primary antibody (Ab_1). One part was to immobilize CEA-Ab_1 and the other part was to immobilize AFP-Ab_1, and the inactive sites on the AuNPs film was sealed by albumin from bovine serum (BSA). Finally, CEA, AFP, and two kinds of ECL nanohybrid−antibody conjugates were successively added dropwise onto their respective GCE/Au/Ab_1 interface region, forming a complete immunosensor and potential-resolved ECL changes for CEA at −0.6 V and AFP at 0.6 V were taken as detection signal (Scheme 1c).

2. EXPERIMENTAL SECTION

2.1. Materials. Human colon CEA, AFP, and their antibody were obtained from Shanghai LincBio Science. $HAuCl_4{\cdot}3H_2O$, *N*,*N*′-di(*N*,*N*-dimethylethylamine)-3,4,9,10-perylenedicarboximide (97%), and bovineserum albumin (BSA) were purchased from Sigma-Aldrich. Uric acid was obtained from Aladdin. Cholesterol was purchased from Shanghai Macklin Biochemical Co., Ltd. Human serum samples were obtained from Liaocheng People's Hospital. Ultrapure water (>18 MΩ) from a Milli-Q Plus system (Millipore) was used to prepare aqueous solutions.

DOI: 10.1021/acsami.9b11416
ACS Appl. Mater. Interfaces 2019, 11, 33676−33683

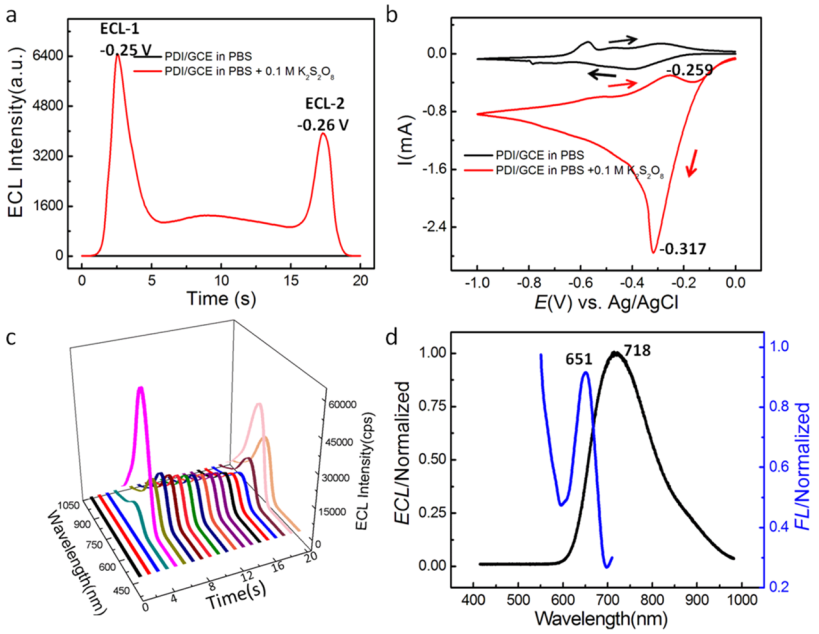

Figure 1. (a) ECL of GCE/PDI in PBS without $K_2S_2O_8$ (dark line) and containing 0.1 M $K_2S_2O_8$ (red line) during cycle potential range from −1 to 0 V. (b) Cyclic voltammetry (CV) of GCE/PDI in PBS without $K_2S_2O_8$ (dark line) and containing 0.1 M $K_2S_2O_8$ (red line). (c) Spooling ECL spectroscopy of GCE/PDI in PBS containing 0.1 M $K_2S_2O_8$ during a CV potential scanning range from −1 to 0 V at 1 s interval. (d) ECL spectra of GCE/PDI at −0.25 V when potential scanning from 0 to −1 V (dark line). Fluorescence (FL) emission spectra (blue line) of PDI powder with 473 nm as the excitation wavelength.

2.2. Synthesis of PDI. The synthesis process and ^{1}H NMR characterization are shown in the Supporting Information.

2.3. Preparation of Potential-Resolved ECL Nanomaterials–Antibody Conjugates. Citrate-reduced AuNPs were prepared according to our previous work. The GO/PDI nanohybrids were prepared by stirring 5 mL of the mixture of PDI (6 mg) and GO (2 mg) solution at 40 °C for overnight. After that, 5 μL of 1 mg mL^{-1} CEA-Ab_2 and 5 μL of 1% BSA solution was added to 1 mL of GO/PDI/AuNPs solution to form GO/PDI/AuNPs/CEA-Ab_2 conjugates. GO/poly(vinylpyrrolidone) (PVP) was prepared according to our previous work. $AgNO_3$, $NaBH_4$, and $HAuCl_4{\cdot}3H_2O$ solutions were in succession added into the GO/PVP solution to form GO/PVP/Au@AgNPs. Then, luminol was added into the GO/PVP/Au@AgNPs solution to form GO/PVP/Au@AgNPs/luminol through Au–N and Ag–N bonds. Finally, AFP-Ab_2 and BSA were added into the GO/PVP/Au@AgNPs/luminol solution to form the GO/PVP/Au@AgNPs/luminol/AFP-Ab_2 conjugates. Here, BSA was used to seal the inactive sites in Au@AgNPs. The details can be found in the Supporting Information.

2.4. Preparation of Multiplex Immunosensor. First, polished GCE was put into phosphate-buffered saline (PBS) solution with 6 mM $HAuCl_4{\cdot}3H_2O$ to electrodeposit AuNPs for 200 s at −0.2 V. Then, a slender tape with 1 mm width was pasted in the middle of the GCE/AuNPs surface. Then, 2.5 μL of 18 μg mL^{-1} CEA-Ab_1 and AFP-Ab_1 each was introduced onto one part of the GCE/Au surface and kept for 12 h at 4 °C to obtain two kinds of GCE/AuNPs/Ab_1 interfaces. Then, 5 μL of 1% BSA was dropped onto the two parts and incubated for 1 h at 37 °C to seal the inactive sites on the AuNPs film. Next, CEA and AFP with different concentrations were dropped onto their respective GCE/Au/Ab_1/BSA interfaces and incubated for 2 h at 37 °C. Finally, 2.5 μL each of GO/PDI/AuNPs/CEA-Ab_2 and GO/PVP/Au@AgNPs/luminol/AFP-Ab_2 was applied to their respective GCE/Au/Ab_1/CEA and GCE/Au/Ab_1/AFP interfaces and incubated for 1 h at 37 °C. After every modification process, the modified electrodes needed be washed by ultrapure water. The prepared sensor was stored at 4 °C for next use.

3. RESULTS AND DISCUSSION

3.1. ECL Mechanism of PDI/$S_2O_8^{2-}$ System. The PDI-modified glass carbon electrode (GCE) displayed dual emissions at −0.25/−0.26 V with $K_2S_2O_8$ as a co-reactant during the cycle potential range from −1 to 0 V (Figure 1a, red line). Control experiments such as the ECL response of bare GCE in the presence of $K_2S_2O_8$ (Figure 3C,a) and PDI-modified GCE in the absence of $K_2S_2O_8$ during the cycle potential ranging from −1 to 0 V (Figure 1a, dark line) were performed to demonstrate the PDI/$S_2O_8^{2-}$ ECL system. There was no ECL response for both situations, indicating that the dual emissions should be due to the co-reaction of $S_2O_8^{2-}$ and PDI, which is different from other perylene derivatives/$S_2O_8^{2-}$ ECL system with single emission and high ECL potential.[9] In addition, ECL response of bare GCE in PBS containing $K_2S_2O_8$, indicating the excited oxygen emission, was avoided between −1 and 0 V (Figure 3C,a).

The cyclic voltammetry (CV) tests were performed to explore the ECL scheme. Perylene derivatives were reported to be two one-electron-transfer redox molecules.[20−22] The CV curve of PDI-modified GCE in the PBS solution without $K_2S_2O_8$ displayed two one-electron-transfer redox peaks at −0.289/−0.393 V (PDI/PDI$^-$) and −0.574/−0.786 V (PDI$^-$/PDI^{2-}) (Figure 1b, dark line). For the CV test of the PDI-modified GCE in the presence of $K_2S_2O_8$, there is a large reduction peak at −0.317 V (Figure 1b, red line), which should be assigned to the first-electron reduction peak of PDI because there is no redox peak for $S_2O_8^{2-}$ on bare GCE between −1 and 0 V (Figure S2, red line). The large increase of PDI reduction current and positive shift of its reduction potential (from −0.393 to −0.317 V) indicated a strong oxygenation between PDI and $K_2S_2O_8$ (Figure 1b, red line).

The ECL rise and fall in the potential dynamic process of PDI during cycle potential scanning range from −1 to 0 V can be observed from the spooling ECL spectra[23,24] shown in

DOI: 10.1021/acsami.9b11416
ACS Appl. Mater. Interfaces 2019, 11, 33676−33683

Figure 1c; every spectra was recorded at 1 s interval. Also, the ECL peak at −0.25 V was located at 717−718 nm (Figure 1d, dark line), which dominated through the whole potential scanning process between −1 and 0 V according to the ECL spectra at different potentials (Figures S3 and S4).

The ultraviolet−visible (UV−vis) spectroscopy of the PDI aqueous solution showed three characteristic absorption peaks of perylene moiety at 469, 499, and 537 nm (Figure S8a, green line).[25] Also, its fluorescence (FL) excitation spectra showed three vibronic bands at 460, 493, and 529 nm (Figure S5, dark line). Compared with the FL excitation spectra, the UV−vis spectra of PDI has a slight red shift (6−9 nm), which could be caused by the aggregation of PDI due to the intermolecular $\pi-\pi$ stacking. Also, there were two emission bands of PDI at 549 and 590 nm, which were attributed to the PDI monomer observed on the FL emission spectra with 493 nm as the excitation wavelength (Figure S5, red line).

Obviously, the ECL wavelength at 717−718 nm did not match with the FL maximum emission peak at 549 nm. The red shifts about 170 nm could be due to the different excited states (monomer and excimer) of PDI. The excimer always emitted emission with a longer wavelength than that of the excited monomer. Thus, the ECL emission should be due to the PDI excimer and the FL emission due to the excited PDI monomer. Due to the strong $\pi-\pi$ interaction among perylene backbones, the perylene derivatives tended to form a dimer in one crystal.[20,26] The dimeric emission band at 651 nm is shown in the FL emission spectra of the PDI powder (Figure 1d, blue line). However, the ECL wavelength at 717−718 nm still red-shifts about 66 nm compared with the dimeric emission band (651 nm). Perylene derivatives were reported to self-organize to H-aggregates through $\pi-\pi$ stacking and J-aggregates through hydrogen bonding.[27] The H- and J-type chromophore packing can mutually transform in a solution as well as in the solid state, and the J-aggregates have a more red-shifted FL emission than the H-aggregates.[28] Thus, the FL dimeric emission band at 651 nm was due to the excited H-dimers and the ECL emission at 717−718 nm due to the excited J-dimers. Thus, the dual ECL emission mechanism of PDI is illustrated in Schemes 2 and S2.[29−31]

In the cathodic process

$$PDI + e^- \rightarrow PDI^{-\bullet} \quad (1)$$

$$PDI^{-\bullet} + S_2O_8^{2-} \rightarrow SO_4^{-\bullet} + PDI \quad (2)$$

Scheme 2. ECL-1 Mechanism of PDI between −0.6 and 0 V and ECL Mechanism of Luminol between 0 and 0.6 V

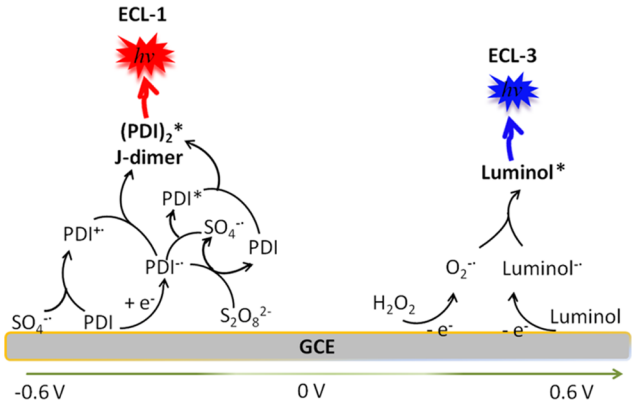

$$PDI + SO_4^{-\bullet} \rightarrow PDI^{+\bullet} + SO_4^{2-} \quad (3)$$

$$PDI^{-\bullet} + SO_4^{-\bullet} \rightarrow PDI^* + SO_4^{2-} \quad (4)$$

$$PDI^* + PDI \rightarrow \text{J-dimer}^* \quad (5)$$

$$PDI^{-\bullet} + PDI^{+\bullet} \rightarrow \text{J-dimer}^* \quad (6)$$

$$\text{J-dimer}^* \rightarrow 2\,PDI + h\nu@717 - 718\ \text{nm} \quad (7)$$

In the anodic process

$$PDI^{2-} - e^- \rightarrow PDI^{-\bullet} \quad (8)$$

$$PDI^{-\bullet} + S_2O_8^{2-} \rightarrow SO_4^{-\bullet} + PDI \quad (9)$$

$$PDI^{-\bullet} - e^- \rightarrow PDI \quad (10)$$

$$PDI + SO_4^{-\bullet} \rightarrow PDI^{+\bullet} + SO_4^{2-} \quad (11)$$

$$PDI^{-\bullet} + SO_4^{-\bullet} \rightarrow PDI^* + SO_4^{2-} \quad (12)$$

$$PDI^* + PDI \rightarrow \text{J-dimer}^* \quad (13)$$

$$PDI^{-\bullet} + PDI^{+\bullet} \rightarrow \text{J-dimer}^* \quad (14)$$

$$\text{J-dimer}^* \rightarrow 2PDI + h\nu@717 - 718\ \text{nm} \quad (15)$$

According to eq 8, the reason for the ECL-2 intensity of PDI at −0.26 V during the anodic process to be smaller than that of ECL-1 at −0.25 V during the cathodic process could be the less PDI^- produced because of the irreversible redox reaction of the PDI molecules, which has been demonstrated by the CV of the PDI-modified GCE in the PBS containing 0.1 M $K_2S_2O_8$ (Figure 1b, red line). Also, the ECL efficiency of the PDI relative to that of $[Ru(bpy)_3]Cl_2/K_2S_2O_8$ was calculated to be 124%, indicating a high ECL efficiency, and the detailed calculation process is shown in the Supporting Information. Luminol was reported to co-react with H_2O_2 and emit a strong ECL at about 0.6 V. Its ECL mechanism is shown in Scheme 2. Thus, PDI and luminol were chosen as two luminophores to prepare potential-resolved ECL nanomaterials.

3.2. Spectroscopic Characterization of GO/PDI/AuNPs ECL Nanomaterial. PDI self-assembled on a GO nanosheet through a $\pi-\pi$ stacking interaction[28] and the formation of the GO/PDI nanomaterial was demonstrated by UV−vis spectra, Fourier transform infrared spectrum, thermogravimetric analysis, and transmission electron microscopy (TEM) images (Figures S8a,b,d, Table S1 and Figure S9). The GO/PDI hybrid further immobilized AuNPs. The N 1s X-ray photoelectron spectroscopy (XPS) peak at 399.7 eV indicated the presence of PDI, and obvious Au 4f peaks at 82.7 and 86.3 eV indicated the presence of AuNPs (Figure 2a). The TEM image of GO/PDI/AuNPs showed round dots well dispersed on the GO/PDI surface, demonstrating the formation of GO/PDI/AuNPs (Figure 2c).

3.3. Spectroscopic Characterization of GO/PVP/Au@AgNPs/Luminol ECL Nanomaterial. Due to their ability to enhance the ECL of luminol/H_2O_2 system, Au@AgNPs were introduced and directly in situ reduced on poly(vinylpyrrolidone) (PVP) modified GO sheets.[32] Luminol immobilized on Au@AgNPs surface through Au−N/Ag−N bonds. The UV−vis spectra (Figure S8c), XPS (Figure 2b), and TEM imaging of GO/PVP/Au@AgNPs/luminol (Figure 2d) were performed. Obvious UV−vis absorbance bands of luminol, round dots of Au@AgNPs shown in TEM, and the N

DOI: 10.1021/acsami.9b11416
ACS Appl. Mater. Interfaces 2019, 11, 33676−33683

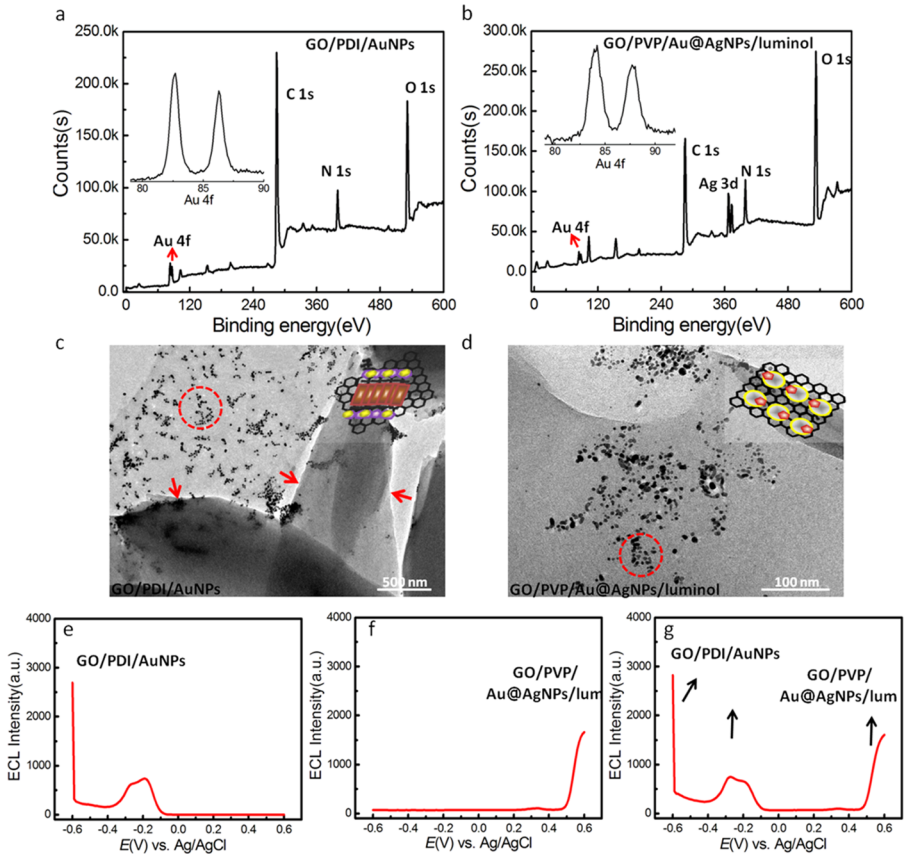

Figure 2. (a) XPS of GO/PDI/AuNPs, inset was the XPS peak of Au 4f. (b) XPS of GO/PVP/Au@AgNPs/luminol, inset was the XPS peak of Au 4f. (c) TEM image of GO/PDI/AuNPs, inset is the schematic diagram of GO/PDI/AuNPs. (d) TEM image of GO/PVP/Au@AgNPs/luminol, inset is the schematic diagram of GO/PVP/Au@AgNPs/luminol. The ECL−voltage curves of GO/PDI/AuNPs (e), GO/PVP/Au@AgNPs/luminol (f), GO/PDI/AuNPs, and GO/PVP/Au@AgNPs/luminol (g) in PBS containing 0.1 M $K_2S_2O_8$ and 5 mM H_2O_2 during the linear scanning potential range from −0.6 to 0.6 V.

1s peak at 399.1 eV, Au 4f peaks at 83.5 and 87.3 eV, and Ag 3d peaks at 367.6 and 373.6 eV in XPS demonstrated the formation of GO/PVP/Au@AgNPs/luminol nanomaterial.

There were strong ECLs at −0.6 V for GO/PDI/AuNPs (Figure 2e) and GO/PVP/Au@AgNPs/luminol at 0.6 V (Figure 2d) in the PBS solution with 0.1 M $K_2S_2O_8$ and 5 mM H_2O_2 during the linear sweep voltammetry (LSV) potential range from −0.6 to 0.6 V. Also, potential-resolved ECL signals were observed at −0.6 and +0.6 V for GO/PDI/AuNPs and GO/PVP/Au@AgNPs/luminol co-modified electrode, and no obvious ECL intensity changes were found for GO/PDI/AuNPs at −0.6 V and for GO/PVP/Au@AgNPs/luminol at 0.6 V, indicating no ECL interference signal existed. These two kinds of ECL nanomaterials were further used to label CEA-Ab_2 and AFP-Ab_2 forming the potential-resolved ECL nanomaterial conjugates as nanoprobes for fabricating a multiplex immunosensor.

3.4. Multiplex Immunosensor's Electrochemical Characterizations. The electrochemical impedance spectroscopy (EIS) of different modified electrodes was performed to demonstrate the successful fabrication of a multiplex immunosensor, and $[Fe(CN)_6]^{3-/4-}$ was chosen as a redox couple.[25] There was a smaller electron transfer resistance (R_{ct}) after AuNPs were electrodeposited on GCE, which was due to the good conductivity of AuNPs (Figure 3B,b). However, a larger R_{ct} was found on the GCE/AuNPs/Ab_1 and GCE/AuNPs/Ab_1/BSA surfaces due to the bad conductivity of the protein layer (Figure 3B,c,d). Also, a much larger R_{ct} is observed on GCE/AuNPs/Ab_1/BSA/CEA@AFP in Figure 3B,e. Finally, a dramatic decrease in R_{ct} was observed when the high conductivity of the ECL nanomaterial−antibody conjugates were captured on the GCE/Au/Ab_1/BSA/CEA@AFP surface (Figure 3B,f).

The ECL behaviors of different modified electrode were also recorded in Figure 3C. However, no ECL was found on bare GCE (Figure 3C,a), GCE/AuNPs (Figure 3C,b), GCE/AuNPs/Ab_1 (Figure 3C,c), GCE/AuNPs/Ab_1/BSA (Figure 3C,d), and GCE/AuNPs/Ab_1/BSA/CEA@AFP (Figure 3C,e), which indicated that the background signal was excluded. Also, the data of a, b, c, d, and e are shown in Figure S10. Also, the potential-resolved ECL from PDI at −0.6 V (ECL-1) and luminol at 0.6 V (ECL-3) were found when ECL nanohybrid−antibody conjugates successfully immobilized on the CEA and AFP recognizing surface (Figure 3C,f), indicating the successful construction of multiplex immunosensors.

3.5. Multiplex Immunosensor's Analytical Performance. The ECL measurements were performed for the fabricated immunosensor at different concentrations of CEA and AFP. The intensity of both ECL peaks (ECL-1 and ECL-3) increased when the concentrations of CEA and AFP increased to 1 ng mL^{-1} (Figure 3D). The peak height of ECL-1 was the detection signal of CEA and ECL-2 peak height was that of AFP. The height of both ECL peaks exhibited a linear response for the logarithm value of CEA concentration (lg

DOI: 10.1021/acsami.9b11416
ACS Appl. Mater. Interfaces 2019, 11, 33676−33683

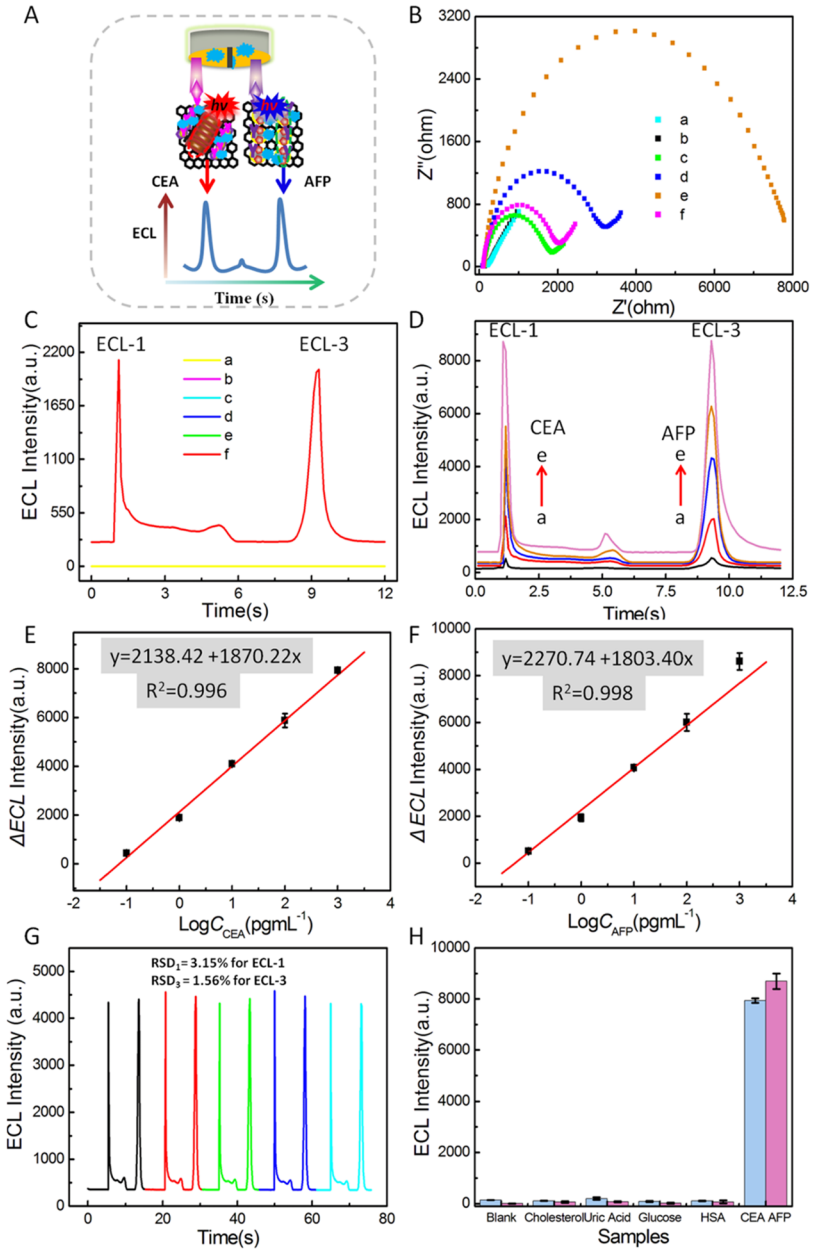

Figure 3. (A) Multiplex immunoassay schematic diagram; the electrochemical impedance spectroscopy (EIS) (B) and ECL-time curves (C) in modification process: (a) bare GCE, (b) GCE/Au, (c) GCE/Au/Ab_1, (d) GCE/Au/Ab_1/BSA, (e) GCE/Au/Ab_1/CEA@AFP, and (f) GCE/Au/Ab_1/CEA@AFP/potential-resolved ECL nanoprobes-Ab_2. (D) ECL−time curves of immunsensor for different CEA and AFP concentrations: (a) 0.1 pg mL^{-1}, (b) 1 pg mL^{-1}, (c) 10 pg mL^{-1}, (d) 100 pg mL^{-1}, and (e) 1000 pg mL^{-1}. (E) Linear response of ECL-1 for log C_{CEA}. (F) Linear response of ECL-3 for log C_{AFP}. (G) Multiplex immunosensor's stability for both C_{CEA} and C_{AFP} at 10 pg mL^{-1}. (H) Multiplex immunosensor's selectivity in different interferences: blank control, 20 mg mL^{-1} cholesterol, 700 mg mL^{-1} uric acid, 20 mg mL^{-1} glucose, 600 mg mL^{-1} human serum albumin (HSA), and 1 ng mL^{-1} for both CEA and AFP.

C_{CEA}) and AFP concentration (lg C_{AFP}) with the range from 0.1 to 1000 pg mL^{-1}. The regression equation for CEA was $\Delta ECL = 2138.42 + 1870.22 \lg C_{CEA}/pg\ mL^{-1}$, and the correlation coefficient (R^2) was 0.996 (Figure 3E, red line) and $\Delta ECL = 2270.74 + 180.40 \lg C_{AFP}/pg\ mL^{-1}$ for AFP and R^2 0.998 (Figure 3F, red line). The detection limit of CEA and AFP was respectively calculated to be 72.73 and 56.09 fg mL^{-1} with 3σ (according to the criterion of IUPAC recommendation).

3.6. Multiplex Immunosensor's Reproducibility, Stability, and Specificity. Three parallel immunosensors were prepared, and their ECL behaviors were recorded to investigate the reproducibility. At the C_{CEA} of 10 pg mL^{-1}, the heights of the ECL peaks of three immunosensors were 3992, 4173, and 4125, respectively, and the relative standard deviation (RSD) was 2.29%. At the C_{AFP} of 10 pg mL^{-1}, the height of the ECL peaks of the three immunosensors were 4031, 4119, and 4053, and the RSD was 1.12%. The results demonstrated good reproducibility of the fabricated multiplex immunosensor. Also, after five cyclic ECL tests, there was no obvious changes on both the ECL-1 and ECL-3 peak height of the fabricated multiplex immunosensor, indicating that the stability of the immunosensor was good (Figure 3G). The multiplex immunosensor's specificity was investigated using

DOI: 10.1021/acsami.9b11416
ACS Appl. Mater. Interfaces 2019, 11, 33676−33683

human serum albumin (HSA), cholesterol, uric acid, and glucose as interferences. Also, the concentration of the interferences was 10 times their normal concentration in the human serum. Thus, the concentration of interference cholesterol was 20 mg mL^{-1}, uric acid was 700 mg mL^{-1}, glucose was 20 mg mL^{-1} and HSA was 600 mg mL^{-1}. The ECL tests of the multiplex immunosensor in the aforementioned concentrations of interferences and 1 ng mL^{-1} for both C_{CEA} and C_{AFP} were performed (Figure 3H). There was much smaller ECL intensity for the immunosensors in interferences than that in CEA and AFP, indicating that the fabricated multiplex immunosensor possessed a high selectivity.

3.7. Practical Application of Multiplex Immunosensor. The multiplex immunosensor's feasibility was investigated by adding various concentrations of CEA and AFP into diluted human serum. Also, the results of both C_{CEA} and C_{AFP} are displayed in Table S2. The acceptable recovery in the range of 99.4−102.8% for CEA and 98.4−100.5% for AFP demonstrated good feasibility for the multiplex immunosensor in human serum.

4. CONCLUSIONS

We reported a new ECL luminophore PDI displaying dual emissions at −0.25/−0.26 V in the $S_2O_8^{2-}$ aqueous system. The wavelength of dual ECL emissions peaked at 717−718 nm, and the ECL was due to the excited J-type PDI dimers, which provided solid bases for low-potential ECL theory studies. Finally, PDI and luminol were taken as potential-resolved luminophores to construct multiplex immunosensor for simultaneous determination of CEA and AFP using LSV technique during potential range from −0.6 to 0.6 V. Also, the multiplex immunosensor showed a sensitive potential-resolved ECL response for CEA at −0.6 V and AFP at 0.6 V with both linear semilogarithmical ranges from 0.1 pg to 1 ng mL^{-1} and good feasibility in human serum. In addition, different from other single-emission luminophores, PDI with dual ECL peaks showed an enticing prospect of built-in self-calibration for a precise quantitative and bioimaging analysis.

■ ASSOCIATED CONTENT

Supporting Information

The Supporting Information is available free of charge on the ACS Publications website at DOI: 10.1021/acsami.9b11416.

Spectroscopy characterization of PDI and potential-resolved ECL nanomaterial−antibody conjugates; multiplex immunosensors' feasibility in human serum; synthesis of PDI; preparation of GO/PDI/AuNPs/CEA-Ab_2 conjugates and GO/PVP/Au@AgNPs/luminol/AFP-Ab_2; ^1H NMR of PDI in CDF_3COOD; ECL spectra of PDI; ECL-2 mechanism of PDI; equation to calculate ECL efficiency of PDI; UV−vis; FTIR spectra of GO, PDI, and GO/PDI; and TGA curve and TEM images of GO, PDI, and GO/PDI (PDF)

■ AUTHOR INFORMATION

Corresponding Authors

*E-mail: weizhanglc@163.com (W.Z.).
*E-mail: hswang@lcu.edu.cn (H.W.).

ORCID

Wei Zhang: 0000-0001-8392-2139

Notes

The authors declare no competing financial interest.

■ ACKNOWLEDGMENTS

The authors greatly thanks Natural Science Foundation of Shandong Province (ZR2017BB084 and ZR2018BB059) and National Natural Science Foundation of China (21804063, 21505063, 21405070, 21375055, and 21427808) provided financial support for this work.

■ REFERENCES

(1) Feng, Y.; Sun, F.; Wang, N. N.; Lei, J. P.; Ju, H. X. $Ru(bpy)_3^{2+}$ Incorporated Luminescent Polymer Dots: Double-Enhanced Electrochemiluminescence for Detection of Single-Nucleotide Polymorphism. *Anal. Chem.* **2017**, *89*, 7659−7666.

(2) Lv, Y.; Chen, S.; Shen, Y.; Ji, J.; Zhou, Q.; Liu, S.; Zhang, Y. Competitive Multiple-Mechanism-Driven Electrochemiluminescent Detection of 8-Hydroxy-2′-deoxyguanosine. *J. Am. Chem. Soc.* **2018**, *140*, 2801−2804.

(3) Chen, L.; Zeng, X.; Si, P.; Chen, Y.; Chi, Y.; Kim, D. H.; Chen, G. Gold Nanoparticle-Graphite-Like C_3N_4 Nanosheet Nanohybrids Used for Electrochemiluminescent Immunosensor. *Anal. Chem.* **2014**, *86*, 4188−4195.

(4) Kitte, S. A.; Gao, W. Y.; Zholudov, Y. T.; Qi, L. M.; Nsabimana, A.; Liu, Z. Y.; Xu, G. B. Stainless Steel Electrode for Sensitive Luminol Electrochemiluminescent Detection of H_2O_2, Glucose, and Glucose Oxidase Activity. *Anal. Chem.* **2017**, *89*, 9864−9869.

(5) Lei, Y. M.; Zhou, J.; Chai, Y. Q.; Zhuo, Y.; Yuan, R. SnS_2 Quantum Dots as New Emitters with Strong Electrochemiluminescence for Ultrasensitive Antibody Detection. *Anal. Chem.* **2018**, *90*, 12270−12277.

(6) Ji, J.; Wen, J.; Shen, Y.; Lv, Y.; Chen, Y.; Liu, S.; Ma, H.; Zhang, Y. Simultaneous Noncovalent Modification and Exfoliation of 2D Carbon Nitride for Enhanced Electrochemiluminescent Biosensing. *J. Am. Chem. Soc.* **2017**, *139*, 11698−11701.

(7) Liu, Y.; Chen, X.; Wang, M.; Ma, Q. A Visual Electrochemiluminescence Resonance Energy Transfer/Surface Plasmon Coupled Electrochemiluminescence Nanosensor for ShigaToxin-Producing *Escherichia Coli* Detection. *Green Chem.* **2018**, *20*, 5520−5527.

(8) Cheng, L.; Liu, X.; Lei, J.; Ju, H. Low-Potential Electrochemiluminescent Sensing Based on Surface Unpassivation of CdTe Quantum Dots and Competition of Analyte Cation to Stabilizer. *Anal. Chem.* **2010**, *82*, 3359−3364.

(9) Xu, L. L.; Zhang, W.; Shang, L.; Ma, R. N.; Jia, L. P.; Jia, W. L.; Wang, H. S.; Niu, L. Perylenetetracarboxylic Acid and Carbon Quantum Dots Assembled Synergistic Electrochemiluminescence Nanomaterial for Ultra-sensitive Carcinoembryonic Antigen Detection. *Biosens. Bioelectron.* **2018**, *103*, 6−11.

(10) Koval'chuk, E. P.; Reshetnyak, O. V.; Chernyak, A. O.; Kovalyshyn, Y. S. Electrochemiluminescence on Np^1-metals: 1. The Analysis of Chemiluminescent Reactions. *Electrochim. Acta* **1999**, *44*, 4079−4086.

(11) Lei, Y. M.; Huang, W. X.; Zhao, M.; Chai, Y. Q.; Yuan, R.; Zhuo, Y. Electrochemiluminescence Resonance Energy Transfer System: Mechanism and Application in Ratiometric Aptasensor for Lead Ion. *Anal. Chem.* **2015**, *87*, 7787−7794.

(12) Xu, S.; Liu, Y.; Wang, T.; Li, J. Positive Potential Operation of a Cathodic Electrogenerated Chemiluminescence Immunosensor Based on Luminol and Graphene for Cancer Biomarker Detection. *Anal. Chem.* **2011**, *83*, 3817−3823.

(13) Ge, L.; Yan, J.; Song, X.; Yan, M.; Ge, S.; Yu, J. Three-Dimensional Paper-based Electrochemiluminescence Immunodevice for Multiplexed Measurement of Biomarkers and Point-of-Care Testing. *Biomaterials* **2012**, *33*, 1024−1031.

(14) Liu, X.; Jiang, H.; Fang, Y.; Zhao, W.; Wang, N. Y.; Zang, G. Z. Quantum Dots Based Potential-Resolution Dual-Targets Electro-

chemiluminescent Immunosensor for Subtype of Tumor Marker and Its Serological Evaluation. *Anal. Chem.* **2015**, *87*, 9163−9169.
(15) Zou, G.; Tan, X.; Long, X.; He, Y.; Miao, W. Spectrum-Resolved Dual-Color Electrochemiluminescence Immunoassay for Simultaneous Detection of Two Targets with Nanocrystals as Tags. *Anal. Chem.* **2017**, *89*, 13024−13029.
(16) Zhou, B.; Zhu, M. Y.; Hao, Y.; Yang, P. H. Potential-Resolved Electrochemiluminescence for Simultaneous Determination of Triple Latent Tuberculosis Infection Markers. *ACS Appl. Mater. Interfaces* **2017**, *9*, 30536−30542.
(17) Guo, W. L.; Ding, H.; Gu, C. Y.; Liu, Y. H.; Jiang, X. C.; Su, B.; Shao, Y. H. Potential-Resolved Multicolor Electrochemiluminescence for Multiplex Immunoassay in a Single Sample. *J. Am. Chem. Soc.* **2018**, *140*, 15904−15915.
(18) Lv, Y.; Zhou, Z.; Shen, Y.; Zhou, Q.; Ji, J.; Liu, S.; Zhang, Y. Coupled Fluorometer-Potentiostat System and Metal-Free Monochromatic Luminophores for High-Resolution Wavelength-Resolved Electrochemiluminescent Multiplex Bioassay. *ACS Sens.* **2018**, *3*, 1362−1367.
(19) Zhou, J.; Nie, L.; Zhang, B.; Zou, G. Z. Spectrum-Resolved Triplex-Color Electrochemiluminescence Multiplexing Immunoassay with Highly-Passivated Nanocrystals as Tags. *Anal. Chem.* **2018**, *90*, 12361−12365.
(20) Mohan Nalluri, S. K.; Zhou, J. W.; Cheng, T.; Liu, Z. C.; Nguyen, M. T.; Chen, T. Y.; Patel, H. A.; Krzyaniak, M. D.; Goddard, W. A.; Wasielewski, M. R.; Stoddart, J. F. Discrete Dimers of Redox-Active and Fluorescent Perylene Diimide-Based Rigid Isosceles Triangles in the Solid State. *J. Am. Chem. Soc.* **2019**, *141*, 1290−1303.
(21) Williams, M. E.; Murray, R. W. Perylene Polyether Hybrids: Highly Soluble, Luminescent, Redox-Active Dyes. *Chem. Mater.* **1998**, *10*, 3603−3610.
(22) Lee, S. K.; Zu, Y.; Herrmann, A.; Geerts, Y.; Müllen, K.; Bard, A. J. Electrochemistry, Spectroscopy and Electrogenerated Chemiluminescence of Perylene, Terrylene, and Quaterrylene Diimides in Aprotic Solution. *J. Am. Chem. Soc.* **1999**, *121*, 3513−3520.
(23) Xiang, G.; Wang, X.; Li, M. S. M.; Lac, K.; Wang, S.; Ding, Z. Probing Excimers of Pt(II) Compounds with Phenyl-1,2,3-Triazolyl and Pyridyl-1,2,4-Triazolyl Chelate Ligands by Means of Electrochemiluminescence. *ChemElectroChem* **2017**, *4*, 1757−1762.
(24) Hesari, M.; Swanick, K. N.; Lu, J. S.; Whyte, R.; Wang, S.; Ding, Z. Highly Efficient Dual-Color Electrochemiluminescence from BODIPY-Capped PbS Nanocrystals. *J. Am. Chem. Soc.* **2015**, *137*, 11266−11269.
(25) Hu, Y.; Wang, K.; Zhang, Q.; Li, F.; Wu, T.; Niu, L. Decorated Graphene Sheets for Label-Free DNA Impedance Biosensing. *Biomaterials* **2012**, *33*, 1097−1106.
(26) Ogawa, T.; Kuwamoto, K.; Isoda, S.; Kobayashi, T.; Karl, N. 3,4:9,10-Perylenetetracarboxylic danhydride (PTCDA) by Electron Crystallography. *Acta Cryst.* **1999**, *B55*, 123−130.
(27) Würthner, F. Perylene Bisimide Dyes as Versatile Building Blocks for Functional Supramolecular Architectures. *Chem. Commun.* **2004**, 1564−1579.
(28) Yagai, S.; Seki, T.; Karatsu, T.; Kitamura, A.; Würthner, F. Transformation from H- to J-Aggregated Perylene Bisimide Dyes by Complexation with Cyanurates. *Angew. Chem., Int. Ed.* **2008**, *47*, 3367−3371.
(29) Chandross, E. A.; Longworth, J. W.; Visco, R. E. Excimer Formation and Emission via the Annihilation of Electrogenerated Aromatic Hydrocarbon Radical Cations and Anions. *J. Am. Chem. Soc.* **1965**, *87*, 3259−3260.
(30) Werner, T. C.; Chang, J.; Hercules, D. M. Electrochemiluminescence of Perylene. The Role of Direct Excimer Formation. *J. Am. Chem. Soc.* **1970**, *92*, 5560−5565.
(31) Grabner, E. W.; Brauer, E. Electrochemiluminescence of Energy-Deficient Systems II. The Role of Excimer Formation in the Pure Perylene System. *Ber. Bunsen Phys. Chem.* **1972**, *76*, 111−114.
(32) Wang, S.; Zhao, Y. Y.; Wang, M. M.; Li, H. J.; Saqib, M.; Ge, C. H.; Zhang, X. D.; Jin, Y. D. Enhancing Luminol Electrochemiluminescence by Combined Use of Cobalt-Based Metal Organic Frameworks and Silver Nanoparticles and Its Application in Ultrasensitive Detection of Cardiac Troponin I. *Anal. Chem.* **2019**, *91*, 3048−3054.

DOI: 10.1021/acsami.9b11416
ACS Appl. Mater. Interfaces 2019, 11, 33676−33683